

# Blue–Green Emitting Phosphor $\text{Ba}_2\text{LiAlSi}_2\text{O}_8\text{:Eu}^{2+}$ for Phosphor-Converted Light-Emitting Diodes via Single-Particle Diagnosis in a Quasi-Quaternary System

Akihiro Nakanishi, Shiro Funahashi, Yukinori Koyama, Hisanori Yamane, Kohsei Takahashi, Takayuki Nakanishi, Naoto Hirosaki, and Takashi Takeda\*



Cite This: *ACS Appl. Mater. Interfaces* 2026, 18, 28857–28865



Read Online

ACCESS |

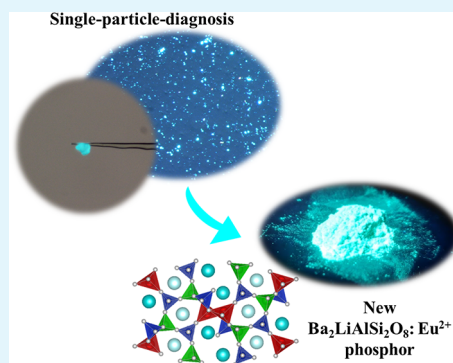
Metrics & More

Article Recommendations

Supporting Information

**ABSTRACT:** Phosphor-converted light-emitting diodes (PC-LEDs) are widely used in various fields due to their long lifetime and high energy efficiency. In particular, blue–green-emitting phosphors have the potential to fill the cyan gap in white LEDs and to be used in display indicators for autonomous driving. A new blue–green-emitting  $\text{Ba}_2\text{LiAlSi}_2\text{O}_8\text{:Eu}^{2+}$  phosphor was discovered through exploratory experiments in the  $\text{BaO}$ – $\text{Li}_2\text{O}$ – $\text{Al}_2\text{O}_3$ – $\text{SiO}_2$  quasi-quaternary system using a single-particle-diagnosis approach. Single-crystal X-ray diffraction analysis revealed that  $\text{Ba}_{1.96}\text{Eu}_{0.04}\text{LiAlSi}_2\text{O}_8$  crystallizes in a space group of  $Pna2_1$  (No. 33) with  $a = 8.04521(11)$  Å,  $b = 19.0484(2)$  Å,  $c = 5.02228(6)$  Å, and  $Z = 4$ . The crystal structure comprises  $\text{LiO}_4$ ,  $\text{AlO}_4$ , and  $\text{SiO}_4$  tetrahedra, which orderly align and form a framework by sharing apical oxygen atoms. Ba atoms are surrounded by eight and seven oxygen atoms in the framework. Density functional theory calculations corroborated the Al and Si arrangement in the  $\text{Ba}_2\text{LiAlSi}_2\text{O}_8$  crystal structure. A single-phase powder of the  $\text{Ba}_2\text{LiAlSi}_2\text{O}_8\text{:Eu}^{2+}$  phosphor was successfully obtained via a solid-state reaction. This phosphor exhibited a blue–green luminescence peak at 497 nm with a full width at half-maximum of 85 nm under 372 nm excitation. The internal and external quantum efficiencies were 51.0% and 42.7%, respectively. The peak intensity at 150 °C was 67% of that at room temperature. We fabricated pc-LEDs based on 405 nm LED chips combined with  $\text{Ba}_2\text{LiAlSi}_2\text{O}_8\text{:Eu}^{2+}$  phosphor, and the CIE chromaticity coordinates were in the blue–green region. These results indicate that the new  $\text{Ba}_2\text{LiAlSi}_2\text{O}_8\text{:Eu}^{2+}$  phosphor is a promising candidate for future LED technologies.

**KEYWORDS:**  $\text{Eu}^{2+}$ -activated phosphor, single-crystal X-ray diffraction, quasi-quaternary system, new crystal phase, phosphor-converted LEDs



## 1. INTRODUCTION

Phosphor-converted light-emitting diodes (pc-LEDs) have applications in various fields due to their advantages of long life and high-energy efficiency.<sup>1–3</sup> A typical example is the combination of blue-LEDs<sup>4</sup> and yellow phosphors to create white light.<sup>5</sup> Color-conversion phosphors are widely studied for various applications. Particularly, yellow-emitting ( $\text{Y}_3\text{Al}_5\text{O}_{12}\text{:Ce}^{3+}$  and  $\text{Ca-Al-Si-Al-O-N}$  ( $\text{Ca}_{m/2}\text{Si}_{12-m-n}\text{Al}_{m+n}\text{O}_n\text{N}_{16-n}\text{:Eu}^{2+}$ )), blue-emitting ( $\text{BaMgAl}_{10}\text{O}_{17}\text{:Eu}^{2+}$ ), and red-emitting ( $\text{CaAlSiN}_3\text{:Eu}^{2+}$  and  $\text{M}_2\text{Si}_2\text{N}_8\text{:Eu}^{2+}$  ( $\text{M} = \text{Ca}, \text{Sr}$ )) phosphors are commercially available for fabricating white LEDs comprising blue or ultraviolet LED chips.<sup>5–9</sup> Narrow-band green phosphor  $\beta\text{-SiAlON:Eu}^{2+}$  ( $\text{Si}_{6-z}\text{Al}_z\text{O}_z\text{N}_{8-z}\text{:Eu}^{2+}$ ) is used in liquid crystal display backlights to enlarge color gamuts.<sup>10,11</sup>

The development of blue–green emitting phosphors, which are used for developing high color-rendering white LEDs to fill cyan gaps, has attracted considerable attention in the advancement of LED applications.<sup>12,13</sup> In addition, blue–

green lights with wavelengths of 440–570 nm exhibit deep penetration depth in marine environments, resulting in their usage for underwater wireless optical communication, fish attractions, and aquaculture in marine ranching systems.<sup>14,15</sup> Recently, turquoise-colored exterior marker lights have been approved by Mercedes-Benz for vehicles equipped with its Drive Pilot SAE (Society of Automotive Engineers) Level 3 automated driving system.<sup>16</sup> Therefore, blue–green emitting phosphors are expected to play a pivotal role in future LED technologies.

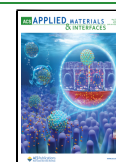
$\text{Eu}^{2+}$ - or  $\text{Ce}^{3+}$ -activated phosphors are attractive for LED applications because of the parity-allowed transition between

**Received:** February 2, 2026

**Revised:** April 30, 2026

**Accepted:** May 6, 2026

**Published:** May 14, 2026



5d- and 4f-orbital.<sup>17</sup> Their luminescence properties are strongly influenced by the local structure surrounding  $\text{Eu}^{2+}$  or  $\text{Ce}^{3+}$ ,<sup>18–21</sup> and this local structure varies with the host material. Therefore, the discovery of suitable host materials is crucial for accelerating phosphor development. However, identifying new host materials remains time-consuming and costly because no clear guidelines for their discovery have been established so far. Traditionally, phosphor development has relied on a trial-and-error approach, typically using known host materials listed in databases (e.g., Inorganic Crystal Structure Database<sup>22</sup>) or by exhaustively screening possible elemental combinations to find new host materials. We previously proposed a single-particle-diagnosis approach that is highly effective for discovering new phosphors.<sup>23</sup> This approach enables the direct determination of the crystal structure and luminescence properties of single-crystal phosphors from multiphase powders containing various secondary phases, without the need for single-phase synthesis. Using this approach, new (oxy)nitride phosphors, such as  $\text{Ba}_5\text{Si}_{11}\text{Al}_7\text{N}_{25}:\text{Eu}^{2+}$ ,  $\text{BaSi}_4\text{Al}_3\text{N}_9:\text{Eu}^{2+}$ ,  $\text{Ba}_2\text{LiSi}_7\text{AlN}_{12}:\text{Eu}^{2+}$ ,  $\text{Sr}_3\text{Si}_{8-x}\text{Al}_x\text{O}_{7+x}\text{N}_{8-x}:\text{Eu}^{2+}$ ,  $\text{Ca}_{1.62}\text{Eu}_{0.38}\text{Si}_5\text{O}_3\text{N}_6$ , and  $\text{Si}_{2.5}\text{Al}_{9.5}\text{O}_{0.5}\text{N}_{12.5}:\text{Eu}^{2+}$ , were discovered.<sup>23–27</sup>

Oxide materials are relatively easy to synthesize; consequently, numerous oxide-based compounds have been reported. To further expand the exploration of oxide materials, exploratory experiments in multicomponent systems combining the single-particle-diagnosis approach offer a more effective strategy for material discovery. In this study, we explored a new oxide-based  $\text{Eu}^{2+}$ -activated phosphor in the  $\text{BaO-Li}_2\text{O-Al}_2\text{O}_3\text{-SiO}_2$  quasi-quaternary system. In previous studies,  $\text{Eu}^{2+}$ -activated phosphors have been discovered in the  $\text{Ba-Li-Al-Si-N}$  system using the single-particle-diagnosis approach.<sup>24</sup>  $\text{Eu}^{2+}$ -doped  $\text{Ba}_2\text{SiO}_4$ ,  $\text{BaAl}_2\text{Si}_2\text{O}_8$ ,  $\text{BaSiO}_3$ ,  $\text{Li}_2\text{BaSiO}_4$ , and  $\text{BaAl}_2\text{O}_4$  have been reported to exhibit blue to yellow emission.<sup>28–32</sup> However, in the oxide-based  $\text{Ba-Li-Al-Si-O}$  system, no new phases have yet been discovered, leaving room for further exploration. A new blue–green emitting  $\text{Ba}_2\text{LiAlSi}_2\text{O}_8:\text{Eu}^{2+}$  phosphor was discovered using the single-particle-diagnosis approach, and a  $\text{Ba}_2\text{LiAlSi}_2\text{O}_8:\text{Eu}^{2+}$  phosphor powder was successfully synthesized for pc-LED application.

## 2. EXPERIMENTAL SECTION

### 2.1. Exploratory Synthesis and Characterization of Particles

Various  $\text{Ba/Eu/Li/Al/Si/O}$  compositions were explored with reagents of  $\text{BaCO}_3$  (99.95%, Kojundo Chemical, Japan),  $\text{Li}_2\text{CO}_3$  (99.99%, Kojundo Chemical, Japan),  $\text{Al}_2\text{O}_3$  (99.99%, TAIMEI CHEMICALS Co., LTD, Japan),  $\text{SiO}_2$  (99.9%, Kojundo Chemical, Japan), and  $\text{Eu}_2\text{O}_3$  (99.9%, Shin-Etsu Chemical Co., LTD, Japan). The mixed precursor powders were calcined on an alumina boat at 1050 °C for 5 h in a reducing atmosphere ( $\text{H}_2:\text{N}_2 = 5:95$  gas). The resulting powders were excited by a 365 nm LED, and a blue–green emitting phosphor particle was collected under microscope observation. Single-crystal X-ray diffraction (XRD) measurements of the particles were performed using a diffractometer (XtaLab Synergy-Custom, Rigaku, Japan) with  $\text{Mo-K}\alpha$  radiation ( $\lambda = 0.71073$  Å). Data were integrated and corrected for absorption using *CrysAlisPro*. The crystal structures were refined by *SHELX*.<sup>33,34</sup> The chemical compositions were analyzed using a scanning electron microscope (Hitachi High-Technology, SU1510) with an energy dispersive spectroscope (EDS, Bruker AXS, XFlash SDD) operated at 10 kV. The excitation and emission spectra of the particles were measured using a self-made device and analyzed using a proximity method.<sup>35</sup>

### 2.2. Density Functional Theory Calculations to Examine Cation Ordering in $\text{Ba}_2\text{LiAlSi}_2\text{O}_8$

Density functional theory (DFT) calculations were performed using the plane-wave basis projector augmented wave method, as implemented in the Vienna *Ab initio* simulation package VASP 6.3.2,<sup>36,37</sup> to examine the arrangement of Li, Al, and Si atoms in  $\text{Ba}_2\text{LiAlSi}_2\text{O}_8$ . The Perdew–Burke–Ernzerhof exchange–correlation functional<sup>38</sup> was used, with the cutoff energy set to 520 eV. Reciprocal-space integration was conducted using a gamma-centered  $2 \times 2 \times 4$  mesh. The total energy converged to  $10^{-9}$  eV/atom. The lattice constants and internal coordinates were optimized until the force converged to 0.01 eV/Å.

### 2.3. Powder Synthesis and Characterization of $\text{Ba}_2\text{LiAlSi}_2\text{O}_8:\text{Eu}^{2+}$

$\text{Ba}_{2(1-x)}\text{Eu}_x\text{LiAlSi}_2\text{O}_8$  ( $x = 0, 0.005, 0.02, 0.04$ , and  $0.06$ ) phosphors were synthesized via a solid-state reaction. The stoichiometric amounts of  $\text{BaCO}_3$ ,  $\text{Li}_2\text{CO}_3$ ,  $\text{Al}_2\text{O}_3$ ,  $\text{SiO}_2$ , and  $\text{Eu}_2\text{O}_3$  were thoroughly mixed in an alumina mortar. After mixing, the precursor powder was calcined in the alumina boat at 1050 °C for 5 h in a reducing atmosphere ( $\text{H}_2:\text{N}_2 = 5:95$  gas). The crystal phases of the phosphors were analyzed at room temperature via powder XRD (SmartLab X-ray Diffractometer, Rigaku, Japan) with  $\text{Cu-K}\alpha_1$  radiation at 45 kV, 200 mA, and  $2\theta$  in the range of  $10^\circ$ – $90^\circ$ . The XRD data were analyzed using Rigaku PDXL 2 software. The luminescence properties of powder samples were measured with a fluorescence spectrometer (FP-8600 Spectrofluorometer, JASCO, Japan), and the decay curves were measured with a fluorescence spectrometer (FLS1000 Spectrofluorometer, Edinburgh Instruments Ltd., UK) under the excitation of a 375 nm pulse laser diode. The internal quantum efficiency (IQE) and external quantum efficiency (EQE) of the phosphors were measured using a QE-2100 system (Otsuka Electronics, Japan).  $\text{BaSO}_4$  was used for a white reference. The cation content was analyzed via inductively coupled plasma optical emission spectroscopy (5800 ICP-OES, Agilent, USA). The measurement solution was prepared by dissolving the sample powder in solution. Sample powder was fused with sodium carbonate and boric acid in a platinum crucible. After cooling, the melt was dissolved in 10 mL of  $\text{HCl}$  (1 + 1) and diluted with water. The solution was transferred to a flask, and Yb standard solution was added as an internal standard. The temperature-dependent luminescence properties were measured using the QE-2100 system combined with a temperature control stage (10002L, Linkam Scientific Instruments, UK).

### 2.4. Characterization of pc-LED with $\text{Ba}_2\text{LiAlSi}_2\text{O}_8:\text{Eu}^{2+}$ Phosphor

The pc-LEDs were fabricated by coating a mixture of the obtained phosphors and silicone resin and with a 405 nm LED chip. Particularly, the obtained phosphors and silicone resin were mixed at a weight ratio of 1:3. The resulting paste mixture was coated on the LED chip and heated at 150 °C for 30 min to cure the resin. The electroluminescence (EL) spectra of the obtained pc-LEDs were measured using the QE-2100 system.

## 3. RESULTS AND DISCUSSION

### 3.1. New Phosphor Discovery

A new oxide phosphor was discovered in the product from a composition of  $\text{Ba/Eu/Li/Al/Si} = 39.2:0.8:10:10:40$ . Figure 1 shows a microscopic photograph of the powder product under 365 nm excitation light. Several particles showed emission in the blue–green region, and some particles with yellow emission were observed.  $\text{Ba}_2\text{SiO}_4$ ,  $\text{BaSiO}_3$ , and  $\text{BaAl}_2\text{Si}_2\text{O}_8$  were identified in the powder XRD analysis (Figure S1). It has been reported that  $\text{Ba}_2\text{SiO}_4:\text{Eu}^{2+}$  and  $\text{BaAl}_2\text{Si}_2\text{O}_8:\text{Eu}^{2+}$  phosphors show blue emission<sup>28,29</sup> and  $\text{BaSiO}_3:\text{Eu}^{2+}$  shows yellow emission.<sup>30</sup> However, some XRD peaks were not consistent with known  $\text{Ba/Li/Al/Si}$ -containing oxides, suggest-

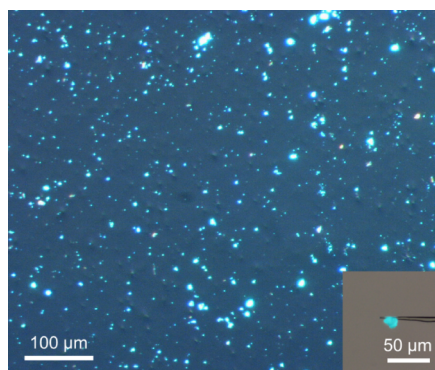


**Figure 1.** Photograph of a powder product from the composition of Ba/Eu/Li/Al/Si = 39.2:0.8:10:10:40 under 365 nm excitation light. The inset shows the selected blue–green luminescent particle for analysis.

ing it is a new compound. In the single-crystal XRD analysis of the emission particles, a new phosphor with blue–green emission was discovered. Figure S2 shows the excitation and emission spectra of blue–green emitting single particles. The monitored excitation spectrum has a broad band in the near-ultraviolet (UV) region, and the emission spectrum shows an emission peak at 491 nm under 350 nm irradiation.

The blue–green emitting particle was determined as a new  $\text{Ba}_2\text{LiAlSi}_2\text{O}_8$  material via the single-crystal XRD analysis. Table 1 lists the crystallographic data and refinement structure parameters. Table 2 lists the fractional coordinates. The Eu occupancy was refined based on the nominal Eu content of 2% relative to Ba, as defined by the starting stoichiometric ratio used in the synthesis. The crystal structure has an orthorhombic system with  $a = 8.04521(11)$  Å,  $b = 19.0484(2)$  Å,  $c = 5.02228(6)$  Å, and a space group of  $Pna2_1$  (No. 33). The reliability factors  $R_1$  and  $wR_2$  were 2.41% and 3.71%, respectively. Table S1 lists the anisotropic displacement parameters. Figure S3 shows the EDS spectrum and analyzed cation ratio of the blue–green emitting single particles. No clear Eu signal was obtained because the amount of Eu is small; thus, it was excluded from the analysis. The atomic ratios of Ba, Al, and Si were 13.6%, 7.2%, and 13.9%, respectively. The cation ratio is in close agreement with the 2:1:2 ratio obtained by single-crystal XRD structural analysis.

Figure 2 shows the crystal structure of  $\text{Ba}_2\text{LiAlSi}_2\text{O}_8$ , drawn using VESTA.<sup>39</sup> The Wyckoff position is only a general  $4a$  site in the space group of  $Pna2_1$ . The crystal structure comprises corner-sharing tetrahedra of  $\text{LiO}_4$ ,  $\text{AlO}_4$ , and  $\text{SiO}_4$ , which are orderly arranged in the framework, and the tetrahedra align along the  $c$  axis.  $\text{SiO}_4$  tetrahedra are isolated with other  $\text{SiO}_4$  tetrahedra in the structure, indicating it is a member of the nesosilicate group. Al and Si often occupied the same crystallographic sites in aluminosilicates; however, Al and Si occupied different crystallographic sites in  $\text{Ba}_2\text{LiAlSi}_2\text{O}_8$ .

To investigate in detail the distribution of Al and Si, which have similar X-ray atomic scattering factors, the cation arrangement at the tetrahedral sites was additionally examined using DFT calculations. Twelve structure models were constructed by placing Li, Al, and Si ions at four tetrahedral sites (T1, T2, T3, and T4). The lattice constants and internal coordinates were optimized via DFT calculations to minimize total energy. Table 3 shows the cation arrangements and relative DFT energies of the four lowest-energy structure models, as well as the  $R_1$  and  $wR_2$  values obtained from the

**Table 1. Crystallographic Data and Structure Refinement Parameters of  $\text{Ba}_{1.96}\text{Eu}_{0.04}\text{LiAlSi}_2\text{O}_8$ <sup>a</sup>**

Formula	$\text{Ba}_{1.96}\text{Eu}_{0.04}\text{LiAlSi}_2\text{O}_8$
Formula mass (g mol <sup>−1</sup> )	493.36
Crystal system	Orthorhombic
Space group	$Pna2_1$ (No. 33)
Temperature (K)	293
$a$ (Å)	8.04521(11)
$b$ (Å)	19.0484(2)
$c$ (Å)	5.02228(6)
$V$ (Å <sup>3</sup> )	769.659(17)
$Z$	4
Radiation type	Mo $K\alpha$
$\mu$ (mm <sup>−1</sup> )	10.727
$\theta$ range for data collection (°)	2.7380 to 38.5940
Index ranges	$-13 \leq h \leq 10, -31 \leq k \leq 31, -8 \leq l \leq 8$
Crystal size (mm)	$0.019 \times 0.017 \times 0.011$
Diffractometer	ROD, Synergy Custom system, HyPix-Arc 150
Absorption correction	Multiscan
$T_{\min}/T_{\max}$	0.827, 1.000
Reflection collected	55852
Independent reflections	3736
Final $R$ indexes [ $I \geq 2\sigma(I)$ ]	$R_1 = 0.0218, wR_2 = 0.0367$
Final $R$ indexes [all data]	$R_1 = 0.0241, wR_2 = 0.0371$
$S$	1.204
$\Delta\rho_{\max}/\Delta\rho_{\min}$ (e Å <sup>−3</sup> )	1.07, −1.40

<sup>a</sup> $R_1, wR_2$  are reliability factors.  $S$  is goodness of fit.  $R_1 = \sum |F_o| - |F_c| / \sum |F_o|$ .  $wR_2 = \{ \sum [w(F_o^2 - F_c^2)^2] / \sum [w(F_o^2)^2] \}^{1/2}$ .  $S = \{ \sum [w((F_o^2 - F_c^2)^2)] / (n - p) \}^{1/2}$ .  $w = 1 / [\sigma^2(F_o^2) + (0.009P)^2 + 1.6987P]$ .  $P = [2F_c^2 + \max(F_o^2, 0)] / 3$ .  $F_o$  is the observed structure factor,  $F_c$  is the calculated structure factor,  $\sigma$  is the standard deviation of  $F_o^2$ ,  $n$  is the number of reflections, and  $p$  is the number of refined parameters.

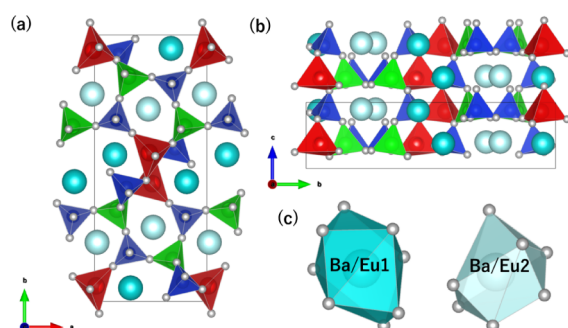
XRD structural analysis. Other cation arrangements were excluded because they had higher relative DFT energies. The lowest-energy arrangement (Li, Al, Si, Si) was identical to the arrangement obtained from the XRD analysis. The arrangement with Li and Al swapped (Al, Li, Si, Si) had the second-lowest energy. However, its energy was 0.997 eV/formula-unit higher than that of the lowest-energy structure. The configuration entropy of a completely random arrangement is  $-4 k_B (0.25 \log 0.25 + 0.25 \log 0.25 + 0.5 \log 0.5) = 0.156$  meV/K formula-unit, where  $k_B$  denotes the Boltzmann constant. This corresponds to an energy of 0.206 eV at 1050 °C. The difference between the lowest and second-lowest energies was significantly larger than the configuration entropy. Therefore, the cations were ordered at the tetrahedral sites, and the degree of disordering should be small. An XRD analysis was also attempted for this cation arrangement, and the  $R_1$  and  $wR_2$  values were unacceptably large. The arrangement with the third-lowest energy was (Li, Si, Si, Al), and the arrangement with the fourth-lowest one was (Li, Si, Al, Si), which had swapped Al and Si compared with the arrangement with the lowest energy. Because Al and Si are difficult to distinguish in an XRD analysis, the  $R_1$  and  $wR_2$  values obtained for these two arrangements were comparable to those of the lowest-energy structure. However, DFT calculations showed higher energies of 1.203 and 1.253 eV/formula-unit for these structures, respectively. Thus, the DFT



**Table 2.** Occupancies, Fractional Atomic Coordinates, and Equivalent Isotropic Atomic Displacement Parameters ( $U_{eq}$ ) of  $Ba_{1.96}Eu_{0.04}LiAlSi_2O_8$ <sup>a</sup>

Atom	Occupancy	<i>x</i>	<i>y</i>	<i>z</i>	$U_{eq}$ (Å <sup>2</sup> )
Ba/Eu1	0.979(3)/0.021(3)	0.18003(3)	0.55048(2)	0.37803(5)	0.00919(4)
Ba/Eu2	0.981(3)/0.019(3)	0.47812(2)	0.72172(2)	0.40001(5)	0.00916(4)
Li	1	0.4870(8)	0.5581(4)	0.8649(18)	0.0119(12)
Al	1	0.80188(13)	0.65697(5)	0.8667(3)	0.00543(18)
Si1	1	0.19239(11)	0.68060(4)	0.8825(3)	0.00532(13)
Si2	1	0.71634(12)	0.57203(5)	0.3649(2)	0.00545(16)
O1	1	0.8616(4)	0.51509(14)	0.3463(6)	0.0122(6)
O2	1	0.6950(4)	0.59328(14)	0.6833(5)	0.0075(5)
O3	1	0.7679(4)	0.64613(15)	0.2089(5)	0.0098(5)
O4	1	0.2222(4)	0.76149(14)	0.7714(6)	0.0094(5)
O5	1	0.5406(4)	0.54571(16)	0.2467(6)	0.0110(5)
O6	1	0.3354(4)	0.63184(15)	0.7611(6)	0.0103(5)
O7	1	0.1888(4)	0.68277(15)	0.2021(5)	0.0096(5)
O8	1	0.0094(4)	0.65832(16)	0.7660(6)	0.0103(5)

$$^a U_{eq} = (1/3)\{U_{11}(aa^*)^2 + U_{22}(bb^*)^2 + U_{33}(cc^*)^2 + 2U_{12}a^*b^*ab \cos \gamma + 2U_{13}a^*c^*ac \cos \beta + 2U_{23}b^*c^*bc \cos \alpha\}.$$

**Figure 2.** Crystal structure viewed from (a) the *c* axis and (b) the *a* axis, and polyhedra of (c) Ba/Eu1- and Ba/Eu2-site of  $Ba_{1.96}Eu_{0.04}LiAlSi_2O_8$ . Black solid line represents the unit cell. Cyan and light cyan spheres are Ba/Eu1 and Ba/Eu2 sites. Red, green, and blue tetrahedra are  $LiO_4$ ,  $AlO_4$ , and  $SiO_4$ . Light gray spheres represent O atoms.**Table 3.** Cation Arrangement at Tetrahedral Sites, Relative Energies Evaluated by DFT Calculations, and XRD Analysis Results for the Four Lowest-Energy Cation Arrangements

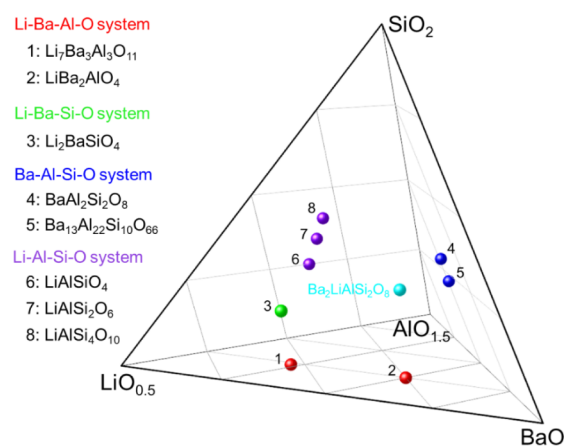
No.	T1	T2	T3	T4	$\Delta E$ (eV/formula-unit)	$R_1$ (%)	$wR_2$ (%)
1	Li	Al	Si	Si	0	2.41	3.71
2	Al	Li	Si	Si	0.997	9.44	23.81
3	Li	Si	Si	Al	1.203	2.46	3.96
4	Li	Si	Al	Si	1.253	2.47	4.01

calculation results were consistent with the ordered cation arrangement obtained via XRD analysis.

Considering the tetrahedral framework of  $Ba_2LiAlSi_2O_8$ , each  $LiO_4$  tetrahedron shares corners with two  $LiO_4$  units, one  $AlO_4$  unit, and four  $SiO_4$  units, whereas each  $AlO_4$  tetrahedron shares corners with one  $LiO_4$  unit and four  $SiO_4$  units. From the electrostatic repulsion viewpoint, the  $LiO_4$  tetrahedron shares corners with a greater number of surrounding tetrahedra than the  $AlO_4$  tetrahedron due to the lower valence state of  $Li^+$ . Ba occupies two polyhedral sites formed by the tetrahedral framework, where the Ba1 and Ba2 sites are coordinated by eight and seven oxygen atoms, respectively. Table S2 summarizes the cation–anion distances and bond valence sums (BVS).<sup>40</sup> The average Ba–O distances for the Ba1 and Ba2 sites are 2.87 and 2.79 Å, respectively. The BVS values for

Ba1 and Ba2 are 1.88 and 1.91, respectively. The average bond lengths of Li–O, Al–O, Si1–O, and Si2–O are 2.00, 1.75, 1.63, and 1.63 Å, respectively. These values correspond to the order of the ionic radii of  $Li^+$  (0.59 Å),  $Al^{3+}$  (0.39 Å), and  $Si^{4+}$  (0.26 Å). The BVS values for the Li, Al, Si1, and Si2 sites are 0.95, 3.07, 3.99, and 3.91, respectively. From the BVS values, it is clearly confirmed that  $Li^+$ ,  $Al^{3+}$ , and  $Si^{4+}$  are orderly arranged at the tetrahedral sites.

The crystal structure of  $Ba_2LiAlSi_2O_8$  is related to those of  $PbZnSiO_4$  (larsenite) and  $PbLiPO_4$ .<sup>41,42</sup> Considering the crystal structure of  $Ba_2LiAlSi_2O_8$  based on that of  $PbZnSiO_4$ , the Pb site is substituted by Ba and the Zn site is orderly substituted by Li and Al in a 1:1 ratio. Based on that of  $PbLiPO_4$ , the Pb site is substituted by Ba and half of the Li site is orderly substituted by Al. The  $PO_4$  unit is substituted by the  $SiO_4$  unit. Figure 3 shows the phase diagram of the BaO–

**Figure 3.** Phase diagram of the BaO–Li<sub>2</sub>O–Al<sub>2</sub>O<sub>3</sub>–SiO<sub>2</sub> quasi-quaternary system.

$Li_2O$ – $Al_2O_3$ – $SiO_2$  quasi-quaternary system.  $Li_7Ba_3Al_3O_{11}$ ,  $LiBa_2AlO_4$  (Li–Ba–Al–O system),  $Li_2BaSiO_4$  (Li–Ba–Si–O system),  $BaAl_2Si_2O_8$  (Ba–Al–Si–O system),  $LiAlSiO_4$ ,  $LiAlSi_2O_6$ , and  $LiAlSi_4O_{10}$  (Li–Al–Si–O system) are known crystal phases of the quasi-ternary system.<sup>43–50</sup> In summary, single-crystal XRD analysis and DFT calculations revealed that a new crystal phase,  $Ba_2LiAlSi_2O_8$ , was identified in the BaO–Li<sub>2</sub>O–Al<sub>2</sub>O<sub>3</sub>–SiO<sub>2</sub> quasi-quaternary system.

### 3.2. Powder Synthesis and Luminescence Properties of $\text{Ba}_2\text{LiAlSi}_2\text{O}_8\text{:Eu}^{2+}$ Phosphors

To evaluate the luminescence properties of powder phosphors and fabricate the prototype of pc-LEDs, powder synthesis was performed based on the  $\text{Ba}_2\text{LiAlSi}_2\text{O}_8\text{:Eu}^{2+}$  composition. Figure 4 shows the powder XRD patterns of

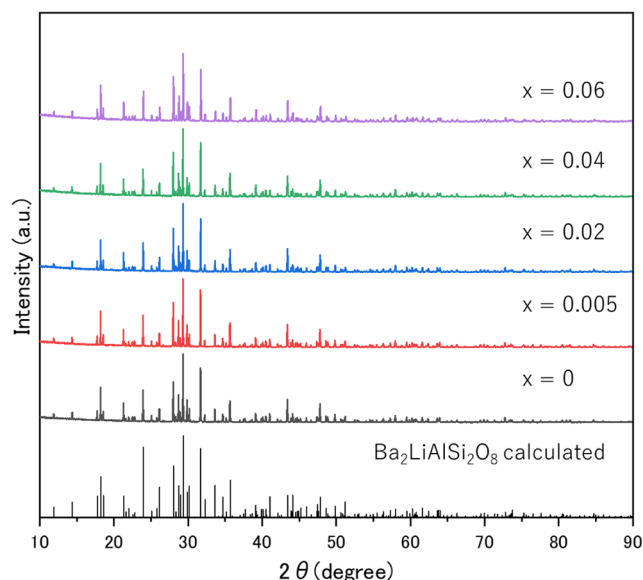


**Figure 4.** XRD patterns of  $\text{Ba}_{2(1-x)}\text{Eu}_{2x}\text{LiAlSi}_2\text{O}_8$  ( $x = 0, 0.005, 0.02, 0.04$ , and  $0.06$ ) phosphors.

$\text{Ba}_{2(1-x)}\text{Eu}_{2x}\text{LiAlSi}_2\text{O}_8$  ( $x = 0, 0.005, 0.02, 0.04$ , and  $0.06$ ). The XRD patterns of all samples are consistent with the diffraction patterns calculated from the crystal structure determined by single-crystal XRD analysis. The crystal phase of  $\text{Ba}_2\text{LiAlSi}_2\text{O}_8$  was mainly obtained in all samples. Figure 5

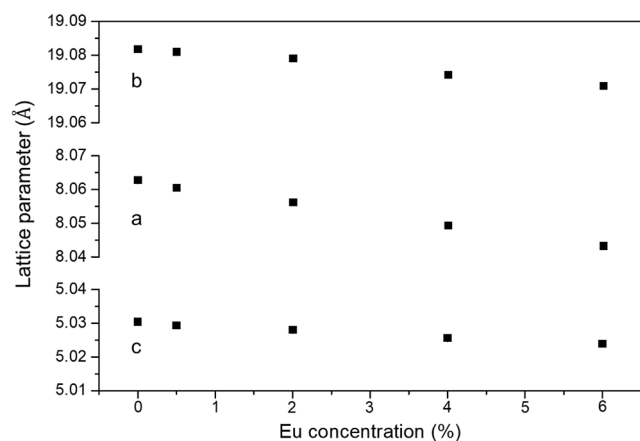


**Figure 5.** Lattice constant of  $\text{Ba}_{2(1-x)}\text{Eu}_{2x}\text{LiAlSi}_2\text{O}_8$  ( $x = 0, 0.005, 0.02, 0.04$ , and  $0.06$ ) phosphors.

shows the lattice parameters of  $\text{Ba}_{2(1-x)}\text{Eu}_{2x}\text{LiAlSi}_2\text{O}_8$  ( $x = 0, 0.005, 0.02, 0.04$ , and  $0.06$ ) phosphors obtained by whole pattern fitting. The linear decrease in the lattice parameters with an increase in Eu content is attributed to the difference in the ionic radii between  $\text{Ba}^{2+}$  ( $r^{\text{VIII}} = 1.42 \text{ Å}$ ) and  $\text{Eu}^{2+}$  ( $r^{\text{VIII}} = 1.25 \text{ Å}$ ),<sup>51</sup> which produces the lattice distortion.<sup>52</sup> Table 4 summarizes the cation contents obtained by ICP analysis. The experimental result ( $\text{Ba:Eu:Li:Al:Si} = 1.91:0.08:1.00:1.00:2.00$ ) corresponds to the theoretical atomic ratio value of  $\text{Ba}_{2(1-x)}\text{Eu}_{2x}\text{LiAlSi}_2\text{O}_8$  ( $x = 0.04$ ).

Figure 6 shows the excitation and emission spectra of  $\text{Ba}_{2(1-x)}\text{Eu}_{2x}\text{LiAlSi}_2\text{O}_8$  ( $x = 0.005, 0.02, 0.04$ , and  $0.06$ )

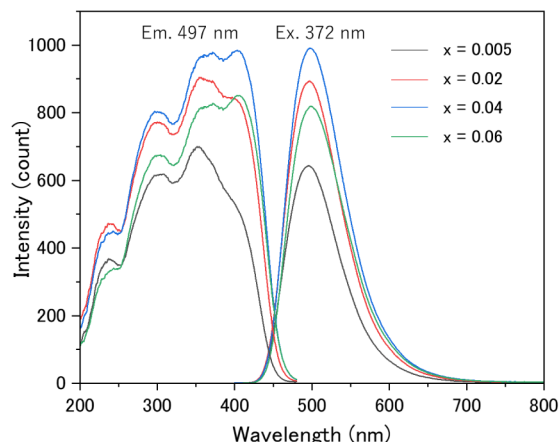


**Figure 6.** Excitation ( $\lambda_{\text{em}} = 497 \text{ nm}$ ) and emission ( $\lambda_{\text{ex}} = 372 \text{ nm}$ ) spectra of  $\text{Ba}_{2(1-x)}\text{Eu}_{2x}\text{LiAlSi}_2\text{O}_8$  ( $x = 0.005, 0.02, 0.04$ , and  $0.06$ ) phosphors.

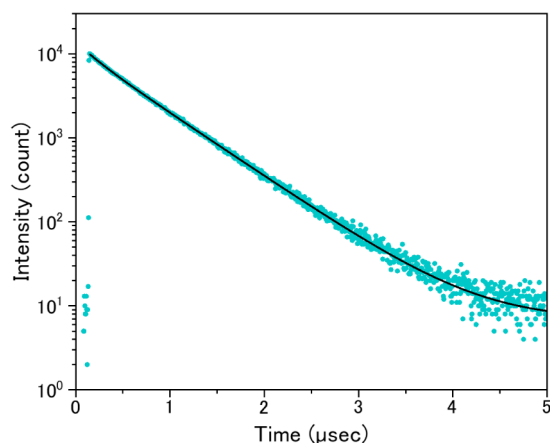
phosphors. The Eu concentration optimized to show the highest intensity was given by  $x = 0.04$ . In the  $x = 0.04$  sample, the broadband excitation spectrum is shown from 200 to 450 nm while the emission spectrum shows a peak at 497 nm with a full width at half-maximum of 85 nm under 372 nm excitation, which originated from the  $5d-4f$  transition of  $\text{Eu}^{2+}$  in the  $\text{Ba}_2\text{LiAlSi}_2\text{O}_8$  host material. With an increase in Eu content, the excitation band intensity at wavelengths longer than 400 nm increased and the emission peak position slightly shifted to longer wavelengths. The excitation and emission intensities gradually increased with Eu content and finally decreased in the sample with  $x = 0.06$  due to the concentration quenching. No significant change in the emission peak was observed for this phosphor even after prolonged UV excitation for 5 h.<sup>53</sup> The IQE and EQE of the  $\text{Ba}_{2(1-x)}\text{Eu}_{2x}\text{LiAlSi}_2\text{O}_8$  ( $x = 0.04$ ) phosphor obtained by 372 nm excitation were 51.0% and 42.7%, respectively.

Figure 7 shows the luminescence decay curve of the  $\text{Ba}_{2(1-x)}\text{Eu}_{2x}\text{LiAlSi}_2\text{O}_8$  ( $x = 0.04$ ) phosphor. The lifetime was obtained by fitting the decay curve with a biexponential function corresponding to two  $\text{Eu}^{2+}$  sites in the crystal

**Table 4.** Cation Composition of  $\text{Ba}_{2(1-x)}\text{Eu}_{2x}\text{LiAlSi}_2\text{O}_8$  ( $X = 0.04$ ) Phosphors by ICP Analysis<sup>a</sup>

	Ba	Eu	Li	Al	Si	O	Total
Theoretical (wt %)	53.4	2.46	1.41	5.46	11.4	25.87	100.0
ICP result (wt %)	52.7	2.43	1.40	5.43	11.3	25.71 <sup>b</sup>	98.9
Mol ratio of ICP result (fixed Al to 1 mol)	1.91	0.08	1.00	1	2.00		

<sup>a</sup>The molar ratio of cation is also listed. <sup>b</sup>This value was calculated from the metal element contents.



**Figure 7.** Measured (light-blue dot) and fitted (black line) decay curves of  $\text{Ba}_{2(1-x)}\text{Eu}_{2x}\text{LiAlSi}_2\text{O}_8$  ( $x = 0.04$ ) phosphor.

structure and a background term. The decay components were determined to be 0.19 and 0.58  $\mu\text{s}$ , with relative weights of 1247 and 8691, respectively. The average decay time was calculated to be 0.56  $\mu\text{s}$ , which is consistent with typical values for the 5d–4f transitions of  $\text{Eu}^{2+}$ .

Figure 8a and b shows the temperature-dependent luminescence spectra and intensity of the  $\text{Ba}_{2(1-x)}\text{Eu}_{2x}\text{LiAlSi}_2\text{O}_8$  ( $x = 0.04$ ) phosphor. Figure S4 shows temperature-dependent normalized luminescence spectra. The photoluminescence intensity gradually decreased with increasing temperature from 25 to 300  $^{\circ}\text{C}$  due to the thermal quenching effect. At 150  $^{\circ}\text{C}$ , the peak and integrated intensities were 67% and 70% of those at room temperature, respectively. There is little difference between changes in peak and integrated intensities, indicating that the peak shape changes slightly. No additional peaks or noticeable peak shifts were observed. These results are favorable for LED applications with no chromatic shift.

### 3.3. Electroluminescence of Blue–Green Emitting pc-LEDs with $\text{Ba}_2\text{LiAlSi}_2\text{O}_8\text{:Eu}^{2+}$ Phosphor

To investigate the potential of the  $\text{Ba}_{2(1-x)}\text{Eu}_{2x}\text{LiAlSi}_2\text{O}_8$  ( $x = 0.04$ ) phosphor, a pc-LED with 405 nm LED chip was fabricated. Figure 9 shows the EL spectrum of the blue–green emitting LED with 405 nm LED chip under forward-bias

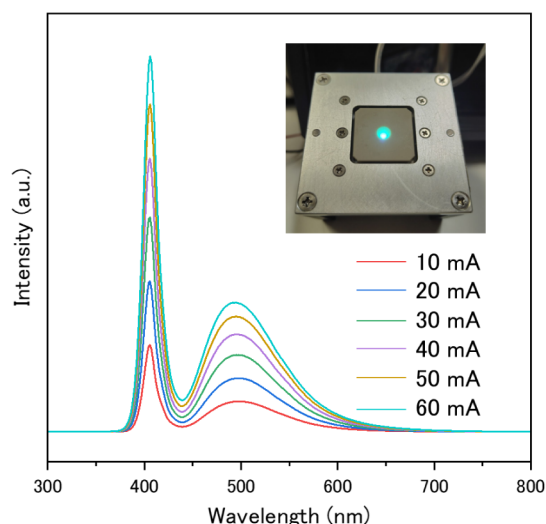


**Figure 9.** EL spectra of blue–green emitting LEDs with 405 nm LED chips and  $\text{Ba}_{2(1-x)}\text{Eu}_{2x}\text{LiAlSi}_2\text{O}_8$  ( $x = 0.04$ ) phosphor. The inset shows the pc-LED emission observed when the current is turned on.

currents from 10 to 60 mA. The inset shows the pc-LED emission when the current is turned on. The EL spectra show the emission band at around 400 nm derived from the LED chip and the blue–green emission band of  $\text{Ba}_2\text{LiAlSi}_2\text{O}_8\text{:Eu}^{2+}$  phosphor at around 500 nm. The CIE chromaticity coordinates of the LED are shown in Figure 10. With an increase in current, the CIE chromaticity coordinates were slightly shifted in the blue–green region. The blue–green phosphor developed in this study has the potential to fill the cyan gap in white LEDs. In addition, the color coordinated for an automated driving system (ADS) marker lamp is regulated in the blue–green region of (CIE  $x$ , CIE  $y$ ) = (0.012, 0.495), (0.200, 0.400), (0.200, 0.320), and (0.040, 0.320) by the SAE. Finally, we emphasized that the novel blue–green  $\text{Ba}_2\text{LiAlSi}_2\text{O}_8\text{:Eu}^{2+}$  phosphor has potential for exterior ADS marker lights and future pc-LED applications.

## 4. CONCLUSION

A new oxide-based blue–green emitting  $\text{Ba}_2\text{LiAlSi}_2\text{O}_8\text{:Eu}^{2+}$  phosphor was discovered using a single-particle-diagnosis approach. The crystal structure, which is related to those of

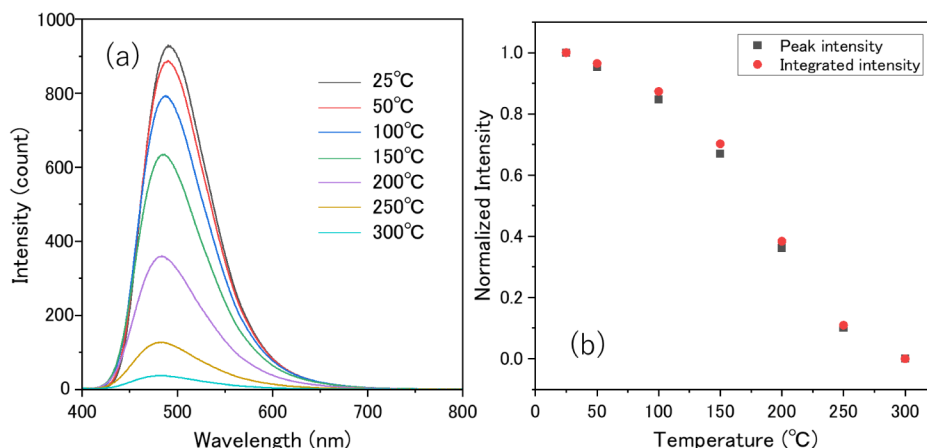


**Figure 8.** (a) Temperature-dependent luminescence spectra, (b) peak and integrated intensities of  $\text{Ba}_{2(1-x)}\text{Eu}_{2x}\text{LiAlSi}_2\text{O}_8$  ( $x = 0.04$ ) phosphor under 372 nm excitation.

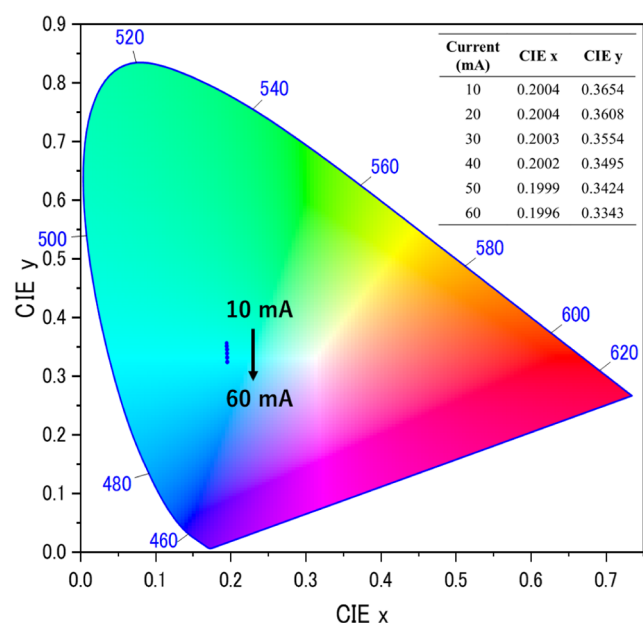


Figure 10. CIE chromaticity coordinates of pc-LED.

PbZnSiO<sub>4</sub> (larsenite) and PbLiPO<sub>4</sub>, was revealed via single-crystal XRD analysis. DFT calculations corroborated the Al and Si arrangement obtained from the single-crystal XRD analysis results. Powder phosphor of Ba<sub>2</sub>LiAlSi<sub>2</sub>O<sub>8</sub>:Eu<sup>2+</sup> was successfully obtained via a solid-state reaction. Ba<sub>2</sub>(1-x)Eu<sub>2x</sub>LiAlSi<sub>2</sub>O<sub>8</sub> (x = 0.04) phosphor showed a blue–green emission under 372 nm excitation. The IQE and EQE were 51.0% and 42.7%, respectively. The peak intensity at 150 °C was 67% of that at room temperature. The EL spectra of the corresponding pc-LEDs showed a blue–green emission band, and the CIE chromaticity coordinates were in the blue–green region regulated by the SAE, indicating that the blue–green emitting Ba<sub>2</sub>LiAlSi<sub>2</sub>O<sub>8</sub>:Eu<sup>2+</sup> phosphor has potential applications in exterior ADS marker lights and future LED technologies. The single-particle-diagnosis approach is effective for discovering new phosphors; thus, it will facilitate the development of pc-LEDs.

## ■ ASSOCIATED CONTENT

### ■ Supporting Information

The Supporting Information is available free of charge at <https://pubs.acs.org/doi/10.1021/acsami.6c02416>.

CIF file (Ba<sub>1.96</sub>Eu<sub>0.04</sub>LiAlSi<sub>2</sub>O<sub>8</sub>) (CIF)

Figure S1: XRD pattern of the powder product of Ba/Eu/Li/Al/Si = 39.2:0.8:10:10:40 calcined at 1050 °C for 5 h in a reducing atmosphere (H<sub>2</sub>:N<sub>2</sub> = 5:95 gas); Figure S2: excitation and emission spectra of the blue–green emitting single particle; Figure S3: EDS spectrum of the blue–green emitting single particle; Figure S4: temperature-dependent normalized luminescence spectra of Ba<sub>2</sub>(1-x)Eu<sub>2x</sub>LiAlSi<sub>2</sub>O<sub>8</sub> (x = 0.04) phosphor under 372 nm excitation; Table S1: anisotropic displacement parameters (Å<sup>2</sup>) of Ba<sub>1.96</sub>Eu<sub>0.04</sub>LiAlSi<sub>2</sub>O<sub>8</sub>; Table S2: bond length, average bond length (Å) and BVS for Ba<sub>1.96</sub>Eu<sub>0.04</sub>LiAlSi<sub>2</sub>O<sub>8</sub> (PDF)

## ■ AUTHOR INFORMATION

### Corresponding Author

Takashi Takeda — Advanced Phosphor Group, National Institute for Materials Science, Tsukuba, Ibaraki 305-0044, Japan; [orcid.org/0000-0003-2510-4562](https://orcid.org/0000-0003-2510-4562); Email: [TAKEDA.Takashi@nims.go.jp](mailto:TAKEDA.Takashi@nims.go.jp)

### Authors

Akihiro Nakanishi — Advanced Phosphor Group, National Institute for Materials Science, Tsukuba, Ibaraki 305-0044, Japan; [orcid.org/0009-0001-1859-261X](https://orcid.org/0009-0001-1859-261X)

Shiro Funahashi — Advanced Phosphor Group, National Institute for Materials Science, Tsukuba, Ibaraki 305-0044, Japan

Yukinori Koyama — Center for Basic Research on Materials, National Institute for Materials Science, Tsukuba, Ibaraki 305-0047, Japan; [orcid.org/0000-0002-7090-4430](https://orcid.org/0000-0002-7090-4430)

Hisanori Yamane — Advanced Phosphor Group, National Institute for Materials Science, Tsukuba, Ibaraki 305-0044, Japan

Kohsei Takahashi — Advanced Phosphor Group, National Institute for Materials Science, Tsukuba, Ibaraki 305-0044, Japan

Takayuki Nakanishi — Advanced Phosphor Group, National Institute for Materials Science, Tsukuba, Ibaraki 305-0044, Japan; [orcid.org/0000-0003-3412-2842](https://orcid.org/0000-0003-3412-2842)

Naoto Hirosaki — Advanced Phosphor Group, National Institute for Materials Science, Tsukuba, Ibaraki 305-0044, Japan

Complete contact information is available at: <https://pubs.acs.org/doi/10.1021/acsami.6c02416>

### Author Contributions

This manuscript was written through the contributions of all authors. All authors have approved the final version of the manuscript.

### Notes

The authors declare no competing financial interest.

## ■ ACKNOWLEDGMENTS

This work was supported by JST, the Core Research for Evolution Science and Technology (grant number JPMJCR19J2). A part of the calculations in this study was performed on the Numerical Materials Simulator at the National Institute for Materials Science.

## ■ REFERENCES

- (1) Schubert, E. F.; Kim, J. K. Solid-State Light Sources Getting Smart. *Science* **2005**, 308, 1274–1278.
- (2) Humphreys, C. J. Solid-State Lighting. *MRS Bull.* **2008**, 33, 459–470.
- (3) Lin, C. C.; Liu, R.-S. Advances in Phosphors for Light-Emitting Diodes. *J. Phys. Chem. Lett.* **2011**, 2, 1268–1277.
- (4) Nakamura, S.; Mukai, T.; Senoh, M. Candela-Class High-Brightness InGaN/AlGaIn Double-Heterostructure Blue-Light-Emitting Diodes. *Appl. Phys. Lett.* **1994**, 64, 1687–1689.
- (5) Xia, Z.; Meijerink, A. Ce<sup>3+</sup>-Doped Garnet Phosphors: Composition Modification, Luminescence Properties and Applications. *Chem. Soc. Rev.* **2017**, 46, 275–299.
- (6) Xie, R.-J.; Hirosaki, N.; Sakuma, K.; Yamamoto, Y.; Mitomo, M. Eu<sup>2+</sup>-Doped Ca- $\alpha$ -SiAlON: A Yellow Phosphor for White Light-Emitting Diodes. *Appl. Phys. Lett.* **2004**, 84, 5404–5406.



- (7) Kim, K.-B.; Kim, Y.-I.; Chun, H.-G.; Cho, T.-Y.; Jung, J.-S.; Kang, J.-G. Structural and optical properties of BaMgAl10O17: Eu<sup>2+</sup> phosphor. *Chem. Mater.* **2002**, *14*, 5045–5052.
- (8) Uheda, K.; Hirosaki, N.; Yamamoto, Y.; Naito, A.; Nakajima, T.; Yamamoto, H. Luminescence Properties of a Red Phosphor, CaAlSiN<sub>3</sub>: Eu<sup>2+</sup> for White Light-Emitting Diodes. *Electrochem. Solid-State Lett.* **2006**, *9*, H22–H25. Luminescence Properties of a Red Phosphor, CaAlSiN<sub>3</sub>: Eu<sup>2+</sup>, for White Light-Emitting Diodes - IOPscience
- (9) Li, Y. Q.; van Steen, J. E. J.; van Krevel, J. W. H.; Botty, G.; Delsing, A. C. A.; DiSalvo, F. J.; de With, G.; Hintzen, H. T. Luminescence Properties of Red-Emitting M<sub>2</sub>Si<sub>5</sub>N<sub>8</sub>: Eu<sup>2+</sup> (M = Ca, Sr, Ba) LED Conversion Phosphors. *J. Alloys Compd.* **2006**, *417*, 273–279.
- (10) Hirosaki, N.; Xie, R.-J.; Kimoto, K.; Sekiguchi, T.; Yamamoto, Y.; Suehiro, T.; Mitomo, M. Characterization and Properties of Green-Emitting  $\beta$ -SiAlON: Eu<sup>2+</sup> Powder Phosphors for White Light-Emitting Diodes. *Appl. Phys. Lett.* **2005**, *86*, 211905.
- (11) Wang, L.; Wang, X.; Kohsei, T.; Yoshimura, K.-I.; Izumi, M.; Hirosaki, N.; Xie, R.-J. Highly Efficient Narrow-Band Green and Red Phosphors Enabling Wider Color-Gamut LED Backlight for More Brilliant Displays. *Opt. Express* **2015**, *23*, 28707–28717.
- (12) Dong, L.; Gao, J.; Guo, Y.; Hou, J.; Shao, B.; Fang, Y. Development of a novel Eu<sup>2+</sup> activated oxonitridosilicate cyan phosphor for enhancing the color quality of a violet-chip-based white LED. *Dalton Trans.* **2024**, *53*, 4175–4184.
- (13) Chen, X.; Huang, X. Full-Visible-Spectrum White LEDs Enabled by a Blue-Light-Excitable Cyan Phosphor. *ACS Appl. Mater. Interfaces* **2024**, *16*, 57365–57376.
- (14) Liu, S.; Wen, D.; Du, R.; Jiang, C.; Chen, J.; Li, J.; Zhou, L.; Molokeev, M. S.; Wu, M. Site-Engineering for Controlling Multiple-Excitation and Emission in Eu<sup>2+</sup>-Activated CaSrSiO<sub>4</sub> Phosphors in Marine Fisheries. *Adv. Optical Mater.* **2023**, *11*, 2195–1071.
- (15) Hua, M.; Liu, S.; Zhou, L.; Bünzli, J.-C.; Wu, M. Phosphor-converted light-emitting diodes in the marine environment: current status and future trends. *Chem. Sci.* **2025**, *16*, 2089–2104.
- (16) *Automated Driving System (ADS) Marker Lamp*; SAE International: Warrendale, PA, 2019.
- (17) Laporte, O.; Meggers, W. F. Some Rules of Spectral Structure. *J. Opt. Soc. Am.* **1925**, *11*, 459–463.
- (18) Pust, P.; Weiler, V.; Hecht, C.; et al. Narrow-Band Red-Emitting Sr[LiAl<sub>3</sub>N<sub>4</sub>]: Eu<sup>2+</sup> as a Next-Generation LED-Phosphor Material. *Nat. Mater.* **2014**, *13*, 891–896.
- (19) Nakanishi, A.; Koyama, Y.; Nakanishi, T.; Funahashi, S.; Yamane, H.; Takahashi, K.; Hirosaki, N.; Ikeno, H.; Takeda, T. Discovery of narrow-band emitting phosphor Na<sub>5</sub>Al<sub>3</sub>F<sub>14</sub>: Eu<sup>2+</sup> using local structure similarity. *J. Alloys Compd.* **2025**, *1010*, 177853.
- (20) Takeda, T.; Koyama, Y.; Ikeno, H.; Matsuishi, S.; Hirosaki, N. Exploring New Useful Phosphors by Combining Experiments with Machine Learning. *Sci. Technol. Adv. Mater.* **2024**, *25*, 1.
- (21) Yang, J.; Zhang, J.; Gao, Z.; Tao, M.; Dang, P.; Wei, Y.; Li, G. Enhanced photoluminescence and thermal stability in solid solution Ca<sub>1-x</sub>Sr<sub>x</sub>Sc<sub>2</sub>O<sub>4</sub>: Ce<sup>3+</sup> ( $x = 0-1$ ) via crystal field regulation and site-preferential occupation. *Inorg. Chem. Front.* **2019**, *6*, 2004–2013.
- (22) *Inorganic Crystal Structure Database (ICSD)*; FIZ Karlsruhe GmbH: Germany, 2022.
- (23) Hirosaki, N.; Takeda, T.; Funahashi, S.; Xie, R.-J. Discovery of New Nitridosilicate Phosphors for Solid State Lighting by the Single-Particle-Diagnosis Approach. *Chem. Mater.* **2014**, *26*, 4280–4288.
- (24) Takeda, T.; Hirosaki, N.; Funahashi, S.; Xie, R.-J. Narrow-Band Green-Emitting Phosphor Ba<sub>2</sub>LiSi<sub>2</sub>AlN<sub>12</sub>: Eu<sup>2+</sup> with High Thermal Stability Discovered by a Single Particle Diagnosis Approach. *Chem. Mater.* **2015**, *27*, S892–S898.
- (25) Wang, X.-J.; Wang, L.; Takeda, T.; Funahashi, S.; Suehiro, T.; Hirosaki, N.; Xie, R.-J. Blue-Emitting Sr<sub>3</sub>Si<sub>8-x</sub>Al<sub>x</sub>O<sub>7+x</sub>N<sub>8-x</sub>: Eu<sup>2+</sup> Discovered by a Single-Particle-Diagnosis Approach: Crystal Structure, Luminescence, Scale-Up Synthesis, and Its Abnormal Thermal Quenching Behavior. *Chem. Mater.* **2015**, *27*, 7689–7697.
- (26) Wang, X.-J.; Funahashi, S.; Takeda, T.; Suehiro, T.; Hirosaki, N.; Xie, R.-J. Structure and luminescence of a novel orange-yellow-emitting Ca<sub>1.62</sub>Eu<sub>0.38</sub>Si<sub>5</sub>O<sub>3</sub>N<sub>6</sub> phosphor for warm white LEDs, discovered by a single-particle-diagnosis approach. *J. Mater. Chem. C* **2016**, *4*, 9968–9975.
- (27) Xu, J.; Funahashi, S.; Takahashi, K.; Nakanishi, T.; Hirosaki, N.; Takeda, T. Cyan-Emitting Sialon-Polytypoid Phosphor Discovered by a Single-Particle-Diagnosis Approach. *ECS J. Solid State Sci. Technol.* **2021**, *10*, 116002.
- (28) Lin, L.; Ning, L.; Zhou, R.; Jiang, C.; Peng, M.; Huang, Y.; Chen, J.; Huang, Y.; Tao, Y.; Liang, H. Site Occupation of Eu<sup>2+</sup> in Ba<sub>2-x</sub>Sr<sub>x</sub>SiO<sub>4</sub> ( $x = 0-1.9$ ) and Origin of Improved Luminescence Thermal Stability in the Intermediate Composition. *Inorg. Chem.* **2018**, *57*, 7090–7096. Site Occupation of Eu<sup>2+</sup> in Ba<sub>2-x</sub>Sr<sub>x</sub>SiO<sub>4</sub> ( $x = 0-1.9$ ) and Origin of Improved Luminescence Thermal Stability in the Intermediate Composition | Inorganic Chemistry
- (29) Sun, L.; Wang, Q.; Zhang, X.; Yang, Z.; Cheng, J.; Sidike, A.; He, J. Phase transition and fluorescence regulation of BaAl<sub>2</sub>Si<sub>2</sub>O<sub>8</sub>: Eu using Ba source. *J. Lumin.* **2020**, *222*, 117058.
- (30) Shen, K.; Zhang, R.; Jin, Y.; Li, Y.; Hu, Y. Inorganic metal oxide material BaSiO<sub>3</sub>: Eu<sup>2+</sup> for convenient 3D X-ray imaging. *J. Lumin.* **2024**, *269*, 120536.
- (31) Pei, Q.; Chen, L.; Du, F.; Xiao, Y.; Peng, J.; Ye, X. Tunable Luminescence of Ce<sup>3+</sup>/Eu<sup>2+</sup> Activated in Single-Phase Li<sub>2</sub>BaSiO<sub>4</sub> Phosphor via Energy Transfer. *ECS J. Solid State Sci. Technol.* **2021**, *10*, 096005.
- (32) Yin, X.; Tian, Y.; Chen, J.; Yi, X.; Jiang, R.; Zhang, D.; Lin, H.; Zhou, S.; Bai, S. Photoluminescence Performance of BaAl<sub>2</sub>O<sub>4</sub>: Eu<sup>2+</sup> Cyan Phosphor Ceramics. *J. Appl. Phys.* **2023**, *133*, 175105.
- (33) Sheldrick, G. SHELXT—Integrated Space-Group and Crystal-Structure Determination. *Acta Crystallogr., Sect. A* **2015**, *71*, 3–8.
- (34) Sheldrick, G. Crystal Structure Refinement with SHELXL. *Acta Crystallogr., Sect. C* **2015**, *71*, 3–8.
- (35) Takahashi, K.; Takeda, T.; Hirosaki, N. Luminescence of single-particle ceramic phosphor by proximity measurement. *Jpn. J. Appl. Phys.* **2023**, *62*, 016510. Luminescence of single-particle ceramic phosphor by proximity measurement - IOPscience
- (36) Kresse, G.; Furthmüller, J. Efficient iterative schemes for ab initio total-energy calculations using a plane-wave basis set. *Phys. Rev. B* **1996**, *54*, 11169.
- (37) Kresse, G.; Joubert, D. From ultrasoft pseudopotentials to the projector augmented-wave method. *Phys. Rev. B* **1999**, *59*, 1758.
- (38) Perdew, J. P.; Burke, K.; Ernzerhof, M. Generalized Gradient Approximation Made Simple. *Phys. Rev. Lett.* **1996**, *77*, 3865.
- (39) Momma, K.; Izumi, F. VESTA 3 for three-dimensional visualization of crystal, volumetric and morphology data. *J. Appl. Crystallogr.* **2011**, *44*, 1272–1276.
- (40) Brese, N. E.; O'Keeffe, M. Bond-valence parameters for solids. *Acta Crystallogr., Sect. B* **1991**, *47*, 192–197.
- (41) Prewitt, C. T.; Kirchner, E.; Preisinger, A. Crystal structure of larsenite PbZnSiO<sub>4</sub>. *Z. Kristallogr.* **1967**, *124*, 115–130.
- (42) Han, G.; Liu, Q.; Wang, Y.; Su, X.; Yang, Z.; Pan, S. Experimental and theoretical studies on the linear and nonlinear optical properties of lead phosphate crystals LiPbPO<sub>4</sub>. *Phys. Chem. Chem. Phys.* **2016**, *18*, 19123–19129.
- (43) Nishita, Y.; Yamane, H. Li<sub>7</sub>Ba<sub>3</sub>Al<sub>3</sub>O<sub>11</sub>: a new supertetrahedral oxide. *Dalton Trans.* **2021**, *50*, 17208–17214.
- (44) Nishita, Y.; Simura, R.; Inaguma, Y.; Yamane, H. LiBa<sub>2</sub>AlO<sub>4</sub>: A new lithium barium aluminate having an oxygen tetrahedral framework. *J. Solid State Chem.* **2023**, *317*, 123654.
- (45) Wu, H.; Zhang, B.; Yu, H.; Hu, Z.; Wang, J.; Wu, Y.; Halasyamani, P. S. Designing Silicates as Deep-UV Nonlinear Optical (NLO) Materials using Edge-Sharing Tetrahedra. *Angew. Chem., Int. Ed.* **2020**, *59*, 8922.
- (46) Gebert, W. Die Kristallstruktur von Ba<sub>13</sub>Al<sub>22</sub>Si<sub>10</sub>O<sub>66</sub>. *Z. Kristallogr.* **1972**, *135*, 437–452.
- (47) Chiari, G.; Gazzoni, G.; Craig, J. R.; Gibbs, G. V.; Louisnathan, S. J. Two Independent Refinements of the Structure of Paracelsian, BaAl<sub>2</sub>Si<sub>2</sub>O<sub>8</sub>. *Am. Mineral.* **1985**, *70*, 969–974.



(48) Tscherry, V.; Schulz, H.; Laves, F. Average and Super Structure of  $\beta$ -Eucryptite ( $\text{LiAlSiO}_4$ ). Part II: Superstructure. *Z. Kristallogr.* **1972**, 135, 175–198.

(49) Cameron, M.; Sueno, S.; Prewitt, C. T.; Papike, J. J. High-Temperature Crystal Chemistry of Acmite, Diopside, Hedenbergite, Jadeite, Spodumene and Ureyite. *Am. Mineral.* **1973**, 58, 594–618.

(50) Effenberger, H. Petalit,  $\text{LiAlSi}_4\text{O}_{10}$ : Verfeinerung der Kristallstruktur, Diskussion der Raumgruppe und Infrarot-Messung. *Tschermaks Mineral. Petrogr. Mitt.* **1980**, 27, 129–142.

(51) Shannon, R. D. Revised effective ionic radii and systematic studies of interatomic distances in halides and chalcogenides. *Acta Crystallogr., Sect. A: Found. Adv.* **1976**, 32, 751–767.

(52) Sreevals, S.; Parvathy, P. A.; Sahoo, K. S.; Das, S. Full-color emitting crystal engineered  $\text{Sr}_3\text{Al}_{1-x}\text{Si}_x\text{O}_{4+x}\text{F}_{1-x}$ :  $\text{Eu}^{2+/3+}$  oxyfluorides for developing bendable lighting composites. *J. Alloys Compd.* **2021**, 880, 160483.

(53) Abraham, M.; Thejas, K. K.; Kunti, A. K.; Amador-Mendez, N.; Hernandez, R.; Duras, J.; Nishanth, K. G.; Sahoo, S. K.; Tchernycheva, M.; Das, S. Strategically Developed Strong Red-Emitting Oxyfluoride Nanophosphors for Next-Generation Lighting Applications. *Adv. Opt. Mater.* **2024**, 12, 2401356.



CAS BIOFINDER DISCOVERY PLATFORM™

# PRECISION DATA FOR FASTER DRUG DISCOVERY

CAS BioFinder helps you identify  
targets, biomarkers, and pathways

Unlock insights

**CAS**  
A division of the  
American Chemical Society